On stable self-pumped phase conjugation in $BaTiO_3$ for high density storage and readout

F. C. Lin and M. A. Fiddy

1991

Department of Electrical Engineering,
University of Massachusetts at Lowell,
Lowell, MA 01854

N00014-89-J-1158

ABSTRACT

We present experimental results and observations on parameters affecting the storage and stable read-out of information based on self-pumped phase conjugation (SPPC) in $BaTiO_3$ (barium titanate). A storage scheme is described which exploits fanning in horizontal planes within the crystal. The stability of SPPC reflectivity is strongly temperature dependent, as well as being dependent on the spatial frequency content of the stored data. The stability of the conjugated signal can be greatly improved by decreasing the temperature of the crystal and by increasing spatial frequency content, for example, by artificially introducing a spatial carrier frequency.

1. Introduction

So-called self-pumped phase conjugation (SPPC) [1] in $BaTiO_3$ crystals has been exploited in various optical devices and device architectures such as interferometers [2], oscillators [3], optical neural networks [4], and dynamic holographic memory storage and processing [5]. Unfortunately, the temporal evolution of the SPPC reflectivity can exhibit instability [6-11] which degrades the quality of stored images or data sets for real-time processing. The physics of the SPPC instability is not well-understood, although possible causes have been reported and attributed to several reasons such as the optical feedback to the laser cavity [7,12] and to the phase-conjugate wave [11], frequency shifts in the phase-conjugate beam [9,11], as well as deterministic chaos [6].

We have studied the temporal evolution of the SPPC intensity $I_{PC}(t)$ in $BaTiO_3$ crystals (obtained from Sanders Associates, Merrimack, NH) as a function of the geometrical parameters that might affect the stability of $I_{PC}(t)$. These geometrical parameters are the incident angle θ, the impact position l on the crystal face, and the distance L between the imaging lens and the impact point (see the insertion in Figure 1). Additional physical parameters affecting the stability of $I_{PC}(t)$ are (1) the spatial frequency content of the information being stored and (2) the temperature change of the crystal either due to the environmental temperature variation or the beam-heating effect, (see next section).

Our objective is to identify optimal conditions in order to stabilize and maximize the SPPC reflectivity $R(t)$ for real-time optical information storage and recall at low laser power. Conventionally, $R(t)$ is defined as the ratio of $I_{PC}(t)$ to the intensity I_M (retro-reflected by a mirror, which replaces the crystal with all of parameters fixed, to the detector). In the SPPC experiments, we

define the optimal condition for $R(t)$ as that $|R_{max} - R(t)|/R_{max} \leq 0.1$ where R_{max} is the maximum value of $R(t)$ (recorded from 10 minutes to 1 hour) and also the maximum value in terms of the above parameters. The storage strategy is based on changing the vertical displacement of the incident information-bearing wave when focused down onto the crystal face; a different vertical position is selected for each new data set. Storage occurs as a result of fanning by the incident beam within the crystal, but this fanning is confined to a horizontal plane; non-interfering storage of multiple information sets is possible in adjacent horizontal planes. Focusing information down to a spot size of a few microns defines the thickness of each information-bearing layer.

2. Experiments and Observations

The top view of the experimental layout is depicted in Figure 1. The incident p-wave (fixed at 514.5 nm in wavelength for all experiments) is collimated and expanded to about 1.5 cm in diameter. To monitor the stability of the laser power P, a 79%-transmission neutral density filter is placed in front of the collimator as the beam splitter. It is found that the amplitude fluctuation of the laser power is no greater than 0.2%. A combination of two polarizers and a tilted quarter-wave plate forms a good isolator which is measured to provide an isolation ratio about 10^4 which minimizes optical feedback to the laser cavity. The collimated beam is, then, passed through a mask (containing the information to be stored) and focused down onto the front face of the crystal. A Michelson interferometer is used to monitor the frequency shift between the incident beam and the SPPC signal. At P = 0.25 W, 0.85 W, and 1 W, we observe frequency shifts as small as 2×10^{-3} Hz, 2.4×10^{-3} Hz, and 2.5×10^{-3} Hz, respectively. Consequently, fluctuations in the SPPC signal due to

beat frequencies would be of this order. Furthermore, the fact that we have measured several stable $I_{PC}(t)$ cases provides the strong evidence of eliminating two possible causes of the SPPC instability: (1) the optical feedback and (2) the frequency shift.

Knowing the thermal conductivity (0.045 W cm^{-1} $°K^{-1}$ measured at room temperature) of the barium titanate sample [13], one could deduce the crystal temperature as a function of the incident intensity I_0 at the entrance face of the crystal. Because of difficulties associated with estimating the heat lost, we measured the temperature changes ΔT (with error magnitudes less than 0.5 °C) for the sample #1359-D. These are plotted in Figure 2 as a function of I_0 at two positions: (1) at the top of the entrance face and (2) at the middle of the top surface of the crystal, when the incident beam is directed at the center of the entrance face. There is approximately a linear variation in the temperature change with increasing I_0. It is interesting to note that at $I_0 \approx 70$ mW/cm^2, the temperature increases as much as 50 °C near the the entry point of the laser beam while it is 29.9 °C at the top (2 mm away from the entry point) of the entrance face. At these intensities, the temperature gradient from the entry point through the crystal is as high as 10 °C per mm. Naturally, this large temperature variation near the entry point will affect, locally, the optical properties of the crystal. Furthermore, since the crystal temperature also changes globally as a result of beam-induced heating, one could expect temperature-dependent changes in optical path within the crystal. These will lead to variations in the interference patterns that arise and which are responsible for the generation of the SPPC.

For some of $I_{PC}(t)$ measurements described below, the laser power is fixed at 25 mW and the incident intensity at the entrance face of the crystal is about 100 μW/cm^2; this induced a 0.9 °C increment of the crystal temperature with

respect to the surroundings. Correspondingly, this temperature increment causes the crystal (with the linear coefficient of thermal expansion about 8.196×10^{-6} °K^{-1}) to expand 0.037 μm in its linear dimension (~ 5 mm each side). Since the refractive index of the extraordinary wave is given by $n_e(\theta) = n_o n_e / \sqrt{n_o^2 \sin^2\theta + n_e^2 \cos^2\theta} = 2.326$ (for $\theta = 70°$, $n_o = 2.404$, and $n_e = 2.316$), the wavelength of the incident beam in the crystal is approximately 221.2 nm. Thus the heat-induced optical path difference is even more significant, amounting to a 17% change. When I_0 is higher, the path-length change is correspondingly higher because the temperature rise of the crystal is larger. Therefore, if the crystal temperature changes for any reason, whether because of heating by the beam or because of fluctuations in the ambient temperature, one can expect small dimensional changes of the medium to disturb interference effects and modulate the temporal behaviour of $I_{PC}(t)$.

The temperature-dependent absorption coefficient for BSO has been discussed previously [14]. Also, the significance of the temperature and the incident intensity on the response time in BSO, BGO, and $BaTiO_3$ has been reported [15,16]. Recently, the band transport model [17] has been extended to include shallow traps [16,18] in order to explain the intensity-dependent absorption and response time. We measured the attenuation coefficients $\alpha_\perp$ (for the polarization of the incident beam perpendicular to the c-axis of the sample #1359-D) and $\alpha_{//}$ (parallel to the c-axis) as functions of I_0 [see Figure 3 where the magnitudes of error bars are less than 0.05 cm^{-1}]. It is shown that $\alpha_\perp$ is approximately a linear function of I_0 ranging from 0.1 mW/cm^2 to 1.22 mW/cm^2 while $\alpha_{//}$ behaves more complicatedly because of the fanning effect.

From the band transport model, the response time τ depends on T^{-1} when the grating wavenumber k is larger than the Debye screening wavenumber k_0 whereas τ is independent on T when k is smaller than k_0 [19]. These

relationships neglect the temperature dependence of the electrical conductivity and the mobility. It is shown tha: the in-phase grating modulation depths in the low-intensity approximation [the first-terms on the right-hand sides of Eqs. (20) and (21) in Ref. 18] are a function of N_E , M_E , k, and k_0 as well as the parameter $\beta/s_T I_0$. The Debye screening wavenumber k_0 is typically 10 μm^{-1} in $BaTiO_3$ [18]. When $k \ll k_0$, the in-phase grating modulation depths depend on T. On the other hand, when $k \gg k_0$, the in-phase grating modulation depths are independent on T. One can conclude that the stability of $I_{PC}(t)$ for the incident beam containing higher spatial frequencies is better than that for the incident beam being a plane wave [see Figure 4b]. In addition, if the spatial frequency content of the information-bearing incident beam increases, the degree of fanning of the beams in $BaTiO_3$ is higher and the local heating arising from these beams is suppressed. This also improves the stability of $I_{PC}(t)$ because the temperature gradients within the crystal drop and, subsequently, the temperature-induced optical path differences decrease. One might therefore expect that actively cooling the crystal or increasing the spatial frequency content of the incident beams, the stability of $I_{PC}(t)$ will be improved.

3. Optimal Recall Condition

Before taking measurements in all experiments, we illuminated the crystals with low incident intensity I_0 for 1/2 hour in order to speed up the response time. We have found that $I_{PC}(t)$ strongly depends on the geometrical parameters, θ, l, and L. For example, when P = 100 mW, T = 10 °C, and L = 9.7 cm (the focal length f of the imaging lens is 10 cm), the optimal crystal orientation consistently occurred at $\theta \approx 70°$ and $l \approx 2$ mm on the 4.8 mm side (parallel to c-axis) for the sample #1359-D (4×4.5×4.8 mm^3), at $\theta \approx 55°$ and $l \approx 2.4$ mm on the 4.2 mm side (parallel to c-axis) for the sample #88-

A (4.2×4.2×5 mm^3), and at $\theta \approx 25°$ and $l \approx 3$ mm on the 4 mm side (parallel to c-axis) for the sample #159-C (4×4.8×5 mm^3). The tolerance range for θ is within $\pm 10°$ from the above optimal value for all crystals but the available range for l (less than ± 0.5 mm from the above optimal value) is very restrictive and slightly different for each crystal. These rather specific combinations of θ and l not only reveal different geometrical constraints imposed on $BaTiO_3$ crystals of different dimensions but also reflect the fact that the variation in the concentration of defect and impurity centers [20] gives rise to distinctive optical properties for individual crystal.

The maximum value of $I_{PC}(t)$ increases as a function of L varied from 8.2 cm to 11.2 cm. Each observation was conducted during a 1/2-hour period for the sample #1359-D at $P = 100$ mW, $T = 10$ °C, $\theta = 70°$, $l = 2$ mm, $f = 10$ cm. The stable pattern of $I_{PC}(t)$ is confined within a narrow ΔL range (less than 0.5 cm) centered at $L = 9.7$ cm. When f is changed to 17 cm and the rest of parameters remain unchanged, $I_{PC}(t)$ is stable over a wider ΔL range. This is because when f is larger, a longer depth of focus is available to induce interaction regions in the crystal for generating stable SPPC. Meanwhile, at this same optimal condition, the response time of the SPPC grating formation and the quality of the SPPC image are also improved for large f.

For some incident beam geometries, the fanning beam can lead to total internal reflection (TIR) ring patterns within the crystal. With an uncollimated Gaussian beam incident on the crystal, we experience the same difficulty of finding a TIR ring as was reported in reference [9]. However, this is not the case when using an image-bearing incident beam with high spatial frequency content. Multiple TIR rings [Figure 4a] form with a wider ΔL range and also $I_{PC}(t)$ oscillates less frequently [Figure 4b]. With multiple TIR rings or multiple fanning directions, the SPPC instability is reduced. Meanwhile, the temperature-

dependent stability can be illustrated by one set of stable $I_{PC}(t)$ data taken at I_0 = 100 $\mu W/cm^2$ (P = 25 mW, T = 24 °C, θ = 70°, L = 9.7 cm, l = 2.5 mm, and f = 17 cm), after the sample #1359-D was cooled at T = 10 °C for a long period of time [Figure 5]. We note that the presence of the mask reduces the laser intensity by 25%. This reduction in the incident intensity associated with a corresponding reduction in the temperature increment of the crystal, is not sufficient to explain the greater stability of the SPPC. Another two sets of $I_{PC}(t)$ data were taken under the same conditions but with I_0 = 400 $\mu W/cm^2$ (P = 200 mW) and I_0 = 800 $\mu W/cm^2$ (P = 200 mW) and these are also stable.

4. Multiple-image Storage and Readout

We have succeeded in demonstrating multiple-image storage and readout via the SPPC in $BaTiO_3$. This was achieved by changing the location of the imaging lens in the vertical direction such that the image-bearing incident beam illuminates the crystal at different heights on its entrance face. It is difficult to store and recall multiple images at the same height on the entrance face, for example, by changing the incident intensity or the incident angle. This is because the beam fanning pattern, which would be induced by another input image, erases previously stored images. Also, by changing the incident angle, a problem for image recall is that the incident beam may not be rotated back to the previous incident angle precisely enough to fulfill the Bragg condition. The angular selectivity in this case is not as simple as that described in the coupled wave theory [21]. When the spatial frequency content of the image-bearing beam has high complexity, the pattern of volume reflection gratings is also very complicated such that the diffraction efficiency drops very rapidly once the incident angle for the image readout deviates slightly from the exact Bragg

angle [22], or there is a temperature related shift of the grating with respect to the incident beam.

After the crystal was translated (e.g., with 1 μm steps) **in the dark** along the direction perpendicular to the incident beam (with a theoretical beam waist ~ 1.5 μm at the impact position on the crystal face) and returned to the same impact position, the stored images were not successfully recalled because of insufficient precision of the micrometer stage. Considering grating formation [23] for two coupled degenerate four-wave mixing (DFWM) interaction regions [24] and using a rectangular box to represent for the interaction region in order to illustrate the geometrical constraints that causes the readout problem; the reason for this is straightforward to see. In Figure 6a, one set of grating planes is constructed by the interference of the probe beam (incident beam) and the write beam (one of the pump beams generated by the corner-cube reflection) in one of the original interaction regions. Whenever there is a slight shift between the new and the original impact positions in the horizontal direction, there is a misalignment between the new and the original interaction regions. Therefore, it is demonstrated in Figure 6b that the new read beam suffers from a critical violation of the Bragg condition. This readout problem can not be relaxed because it demands an apparatus with translation resolution better than the smallest grating period stored in the crystal. On the other hand, the stored images can be **easily** recalled by changing the vertical location of the imaging lens and returning **almost** to the same impact position even with a lower precision mount. Geometrically, it is shown in Figure 6c that the new read beam satisfies exactly the Bragg reflection even though there is a slight displacement between the new and the original impact positions in the vertical direction. We have noted that the SPPC image-reconstruction time is longer

than a few seconds after being erased and the SPPC image-readout time is of the order of milli-second.

Another two interesting situations are also observed during mechanical disturbance of the crystal. Firstly, one can recall the stored image when the crystal is linearly translated **in the dark** along the incident beam direction to another position which is within ±1 mm of the original position. Beyond this translation range, the beam diameter is enlarged more than ± 0.2 mm and the fanning pattern deviates too much from the original one. Hence, the same situation as described in Figure 6b occurs and the SPPC image readout fails. Secondly, the SPPC image remains intact if the crystal is moved slowly (but still confined within ±1 mm of the original position) along the incident direction. This requires a translation rate slower than 1/6 millimeter per second when the incident beam is on during this translating procedure. It is attributed to the fact that, at a translation speed greater than 0.34 mm/s, the incident beam wanders around the original impact position due to the mechanical disturbance and generates the flux of scanning light to erase the original SPPC image.

5. Temporal Behaviours of the SPPC Intensity

We measured how the reflectivity of the SPPC varies as a function of incident power. The reflectivity was measured at 10 minute intervals and plotted for three different input beam profiles; this is shown in Figure 7. We observe some dependence of R_{max} on the laser power P, but there is no systematic trend in behavior with no mask present. There is a reduction in reflectivity with the USAF test chart mask in place. One can only conjecture that this might be due to the higher spatial frequency content resulting in less storage at deeper traps, leading in turn to decreased storage times at the increased temperatures associated with higher illuminating powers.

In all temporal measurements of $I_{PC}(t)$ for the sample #1359-D, the parameters P, θ, L, l, and f were fixed at 25 mW, 70°, 16.6 cm, 2.5 mm, and 17 cm, respectively. Each measurement of $I_{PC}(t)$ was taken at 5-second interval in order to ensure sufficient sampling of the fluctuation pattern. In Figure 8a, we illustrate a strong temperature dependence; $I_{PC}(t)$ is more stable at T = 10 °C than at T = 18 °C. To verify our conjecture that local crystal heating by the incident laser beam can produce the same effect on $I_{PC}(t)$ as the ambient temperature does, we intentionally exposed the crystal at minimum laser power for almost 6 hours at the same ambient temperature T = 10 °C to raise its temperature and reach stable equilibrium. We obtained a similar behaviour for $I_{PC}(t)$ [Figure 8b] as that shown in Figure 8a. When a tilted neutral density filter (with 79% transmission) was placed in front of crystal, (originally to monitor the stability of the laser power), $I_{PC}(t)$ at I_0 = 100 $\mu W/cm^2$ (P = 25 mW) became even more stable [the thick curve in Figure 5]. This stability has also persisted for ≈ 20 minutes at another two different incident intensities I_0 = 400 $\mu W/cm^2$ (P = 200 mW) and I_0 = 800 $\mu W/cm^2$ (P = 200 mW), before crystal heating resulted in the resumption of instability. The spatial frequency modulation of the incident beam, arising from reflections within the neutral density filter is responsible for the stable behaviour of $I_{PC}(t)$. This can be regarded as the imposition of a carrier wave.

The transition of $R(t)$ from steady → quasi-periodic → chaotic → steady was observed when the impact position l was varied from 0 mm to 1 mm on the entrance face of the crystal [8]. The value of $R(t)$ (≤ 10%) in reference [8] can be improved if the geometrical and physical parameters are optimized. As mentioned above, we have investigated more extensively the parametric dependence of $I_{PC}(t)$ and observed that even at the optimal condition, either quasi-periodic or chaotic pulsation would occasionally occur. In the absence of

thermal effects, we consider that the quasi-periodic pulsation is caused by the energy exchange either between $I_{PC}(t)$ and the accompanied TIR rings or between the beam fanning pattern and the self-pumped channels [25]. It is noted that the TIR ring intersects two regions with the main beam [Figure 4a]. By two-wave mixing theory, the direction of energy coupling at one of these regions is always opposite to that at the other one. Therefore, at the intersection near the entrance position, the energy of the main beam (with higher energy) is coupled to the TIR ring and at the intersection near the exit position, the energy of the TIR ring is coupled to the main beam. Since the amount of energy coupling near the entrance position is more than that near the exit position, the net outcome is that the TIR ring gains the energy. The energy coupling process continues until the condition of the total internal reflection fails due to the intensity-dependency of the local refractive index change and the TIR ring disappears. Subsequently, the whole process repeats again and $I_{PC}(t)$ oscillates quasi-periodically. The oscillating period depends on the rate of the TIR ring build-up process and the rate of energy exchange between the main beam and the TIR ring. Experimentally, we observed that whenever the TIR ring undergoes the rhythmic oscillation, $I_{PC}(t)$ also pulsates accordingly. A single-frequency wave is less stably trapped in a self-induced dielectric waveguide (i.e., the self-pumped channel) [26], than if two or more beams of different frequency were present; one beam providing a measure of guidance for the other. With unstable guiding, the energy can be exchanged, quasi-periodically, between the beam fanning pattern and the self-pumped channel. Experimentally, we also observed the flip-flop process that the clear beam fanning pattern faded into several concentrated channels and, then, those channels dimmed out gradually and the original beam fanning pattern appeared again. As for the

chaotic pulsation of $I_{PC}(t)$, we believe that the random fluctuation of the optical path change due to the thermal effect plays the major role.

6. Conclusion

We have presented experimental results related to the storage and stable recall of information stored in photorefractive barium titanate; readout of this information is by self-pumped phase conjugation, which permits an associative recall to be realized. Our experiments suggest that the temporal behaviour of the SPPC reflectivity depends on several parameters. There is a strong temperature dependence and cooling can restore stability. Also, the SPPC can be stabilized when an optimal incidence condition for an individual $BaTiO_3$ crystal can be specified; the information to be stored is focused onto the crystal face at this optimal position and angle. Finally, the stability of the SPPC reflectivity is improved as the spatial frequency content of the incident beam is increased.

For multiple-image storage and readout, we used the vertical height of the crystal, storing information in adjacent horizontal layers within the body of the crystal. There is minimal overlap between these layers and we have successfully stored distinct images in this way, with a separation between input locations of 20 μm. We project that in a 5 mm cube of material, one could store approximately 200 high resolution images in this fashion. We postulate that the chaotic SPPC instability arises from the fluctuation in the optical paths within the material, which is determined by the local and ambient temperature, which in turn depends on the fanning geometry within the crystal. The fanning patterns are largely determined by the impact position and incidence angle as well as the spatial frequency content of the information-bearing incident beam.

Acknowledgement

We would like to thank T. Yang for taking the frequency shift measurement.

The authors acknowledge the support of ONR Grant N00014-89-J-1158.

References

1. J. Feinberg, Opt. Lett., 7, 486 (1982).
2. J. Feinberg, Opt. Lett., 8, 569 (1983); A. E. Chiou and P. Yeh, Opt. Lett., 11, 306 (1986); M. Serwe, A. Herden, and T. Tschudi, SPIE Vol. 1017, 180 (1988).
3. R. A. McFarlane and D. G. Steel, Opt. Lett., 8, 208 (1983); B. Fischer, S. Sternklar, and S. Weiss, IEEE J. Quant. Electr., 25, 550 (1989).
4. Y. Owechko, O.S.A. Opt. Comp. Digest, Salt Lake City, March, MD4-1, 44 (1989); Y. Owechko, and B. H. Soffer, Opt. Lett., 16, 675 (1991).
5. K. H. Fielding, S. K. Rogers, M. Kabrisky, and J. P. Mills, Opt. Eng., 28, 849 (1989); L. Pugliese and G M. Morris, Opt. Lett., 15, 338 (1990); A. P. Ghosh and R. R. Dube, Opt. Comm., 77, 135 (1990).
6. P. Narum, D. J. Gauthier, and R. W. Boyd, in Optical Bistability III, H. M. Gibbs, P. Mandel, N. Peyghambarian, and S. D. Smith, eds., Springer-Verlag, Berlin, 298 (1986); D. J. Gauthier, P. Narum, and R. W. Boyd, Phys. Rev. Lett., 58, 1640 (1987).
7. M. C. Gower and P. Hribek, J. Opt. Soc. Am., B5, 1750, (1988).
8. A. M. C. Smout, R.W. Eason and M. C. Gower, Opt. Comm., 59, 77 (1986).
9. A. V. Nowak, T. R. Moore, and R. A. Fisher, J. Opt. Soc. Am., B5, 1864 (1988).
10. G. J. Dunning, D. M. Pepper, and M. B. Klein, Opt. Lett., 15, 99 (1990).
11. P. Günter, E. Voit, M. Z. Zha, and J. Albers, Opt. Comm., 55, 210 (1985).
12. F. C. Jahoda, P. G. Weber, and J. Feinberg, Opt. Lett., 9, 362 (1984).
13. Thermal Conductivity: Nonmetallic Solids, Thermophysical Properties of Matter, The TPRC Data Series, Vol. 2, 257, IFI/Plenum, New York-

Washington, (1970).

14. C. Uhrich and L. Hesselink, Opt. Lett., 15, 455 (1990).
15. M. A. Powell and C. R. Petts, Opt. Lett., 11, 36 (1986); D. Rytz, M. B. Klein, R. A. Mullen, R. N. Schwartz, G. C. Valley, and B. A. Wechsler, Appl. Phys. Lett., 52, 1759 (1988).
16. G. A. Brost, R. A. Motes, and J. R. Rotge, J. Opt. Soc. Am., B5, 1879 (1988); D. Mahgerefteh and J. Feinberg, Phys. Rev. Lett., 64, 2195 (1990); G. A. Brost and R. A. Motes, Opt. Lett., 15, 1194 (1990).
17. N. V. Kukhtarev, V. B. Markov, S. G. Odulov, M. S. Soskin, and V. L. Vinetskii, Ferroelectrics, 22, 949 (1979); J. Feinberg, D. Heiman, A. R. Tanguay Jr., and R. W. Hellwarth, J. Appl. Phys., 51, 1297 (1980); Erratum, ibid, 52, 537 (1981); G. C. Valley, Appl. Opt., 22, 3160 (1983).
18. P. Tayebati and D. Mahgerefteh, J. Opt. Soc. Am., B8, 1053 (1991).
19. R. A. Mullen, in Photorefractive Materials and Their Applications I, P. G. Günter and J.-P. Huignard, eds., Springer-Verlag, Berlin, 191-192, (1988).
20. M. B. Klein, in Photorefractive Materials and Their Applications I, P. G. Günter and J.-P. Huignard, eds., Springer-Verlag, Berlin, 195-236 (1988).
21. H. Kogelnik, Bell System Tech. J., 48, 2909 (1969).
22. A. M. Glass, Opt. Eng., 17, 470 (1978).
23. D. M. Pepper, Opt. Eng., 21, 156 (1982).
24. K. R. MacDonald and J. Feinberg, J. Opt. Soc. Am., 73, 548 (1983).
25. D. Wang, Z. Zhang, X. Wu and P. Ye, J. Opt. Soc. B7, 2289 (1990).
26. R. Y. Chiao, E. Garmire, and C. H. Townes, Phys. Rev. Lett., 13, 479 (1964); Erratum, ibid, 14, 1056 (1965).

FIGURE CAPTIONS

Figure 1. Top view of experimental layout; (insertion) the relationship of geometrical parameters.

Figure 2. Graph of the temperature changes ΔT at two positions on the crystal surface as functions of the incident intensity.

Figure 3. Plot of the attenuation coefficients as functions of incident intensity.

Figure 4. (a) photograph displays beam fanning pattern and TIR rings in $BaTiO_3$ when the incident beam is coded with US Air Force resolution chart and (b) the comparison of $I_{PC}(t)$ temporal fluctuations for the incident beam carries with no mask and with US Air Force resolution chart, respectively.

Figure 5. The thin and thick curves are for $I_{PC}(t)$ measured without and with the neutral density filter to monitor the laser power, respectively. The thick curve indicates the evidence of the spatial frequency modulation by the 79%-transmission neutral density filter; the reflectivity of the SPPC is also stabilized at much higher incident powers (≈ an order of magnitude greater) with the neutral density filter in place.

Figure 6. (a) One set of original grating planes stored in one of interaction regions, (b) horizontal misalignment of the new and the original interaction regions, and (c) vertical shift between the new and the original interaction regions.

Figure 7. R_{max} as a function of laser power for incident beams with Gaussian intensity profile (open circles and solid circles on two different days but the same ambient temperature) and with US Air Force resolution chart (open triangles), respectively.

Figure 8. (a) Data of $I_{PC}(t)$ at two different temperatures 10 °C and 18 °C and

(b) Data of $I_{PC}(t)$ indicates the local crystal-heating effect: the thick curve is the same as that in (a) and the thin curve is measured at the same ambient temperature 10 °C but after the crystal was illuminated at low intensity for 6 hours, rendering it unstable once more.

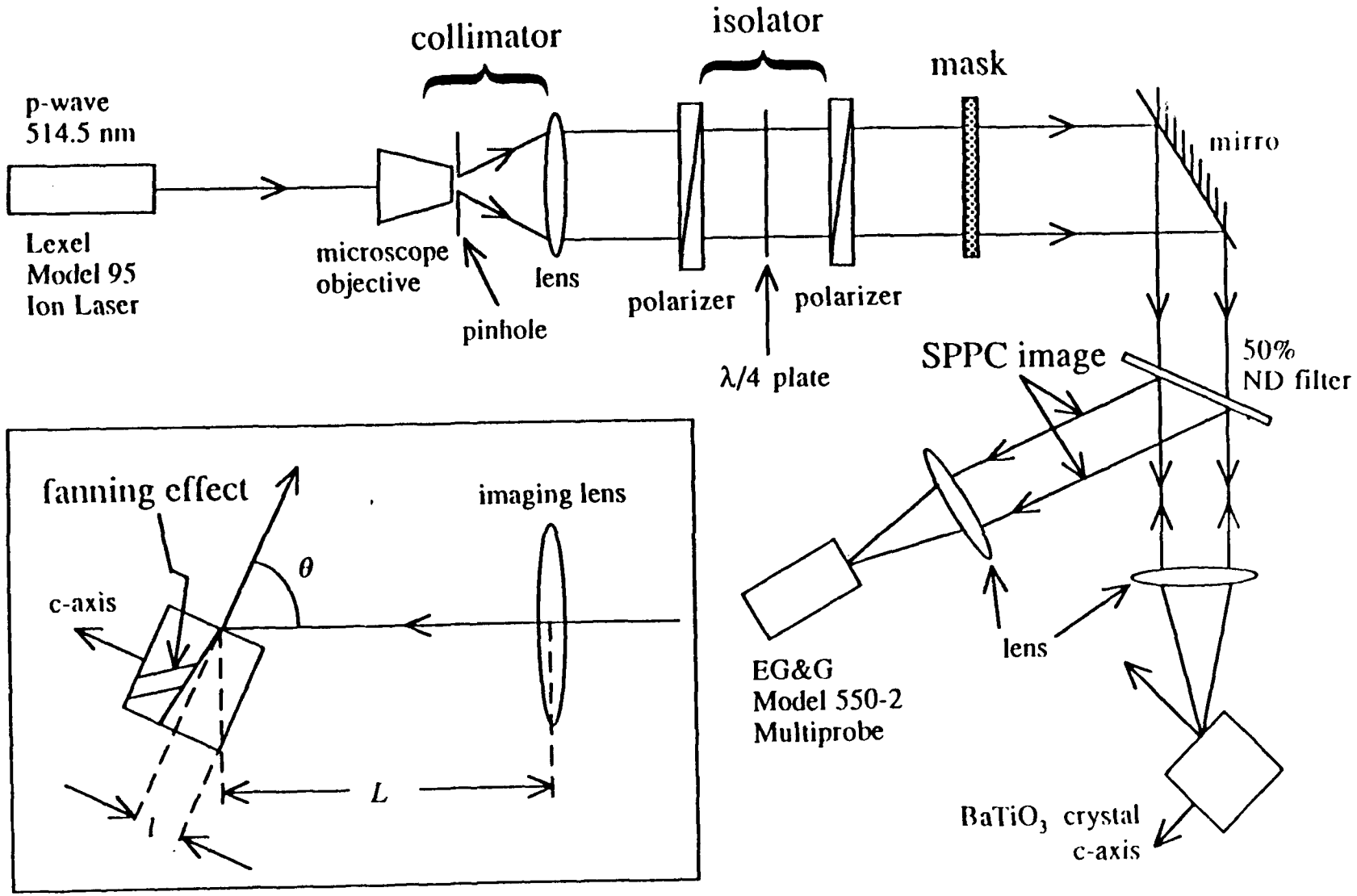
collimator
isolator
mask
p-wave
514.5 nm
Lexel
Model 95
Ion Laser
microscope
objective
lens
pinhole
polarizer
polarizer
λ/4 plate
mirro
SPPC image
50%
ND filter
fanning effect
imaging lens
θ
c-axis
L
EG&G
Model 550-2
Multiprobe
lens
BaTiO3 crystal
c-axis

Figure 1

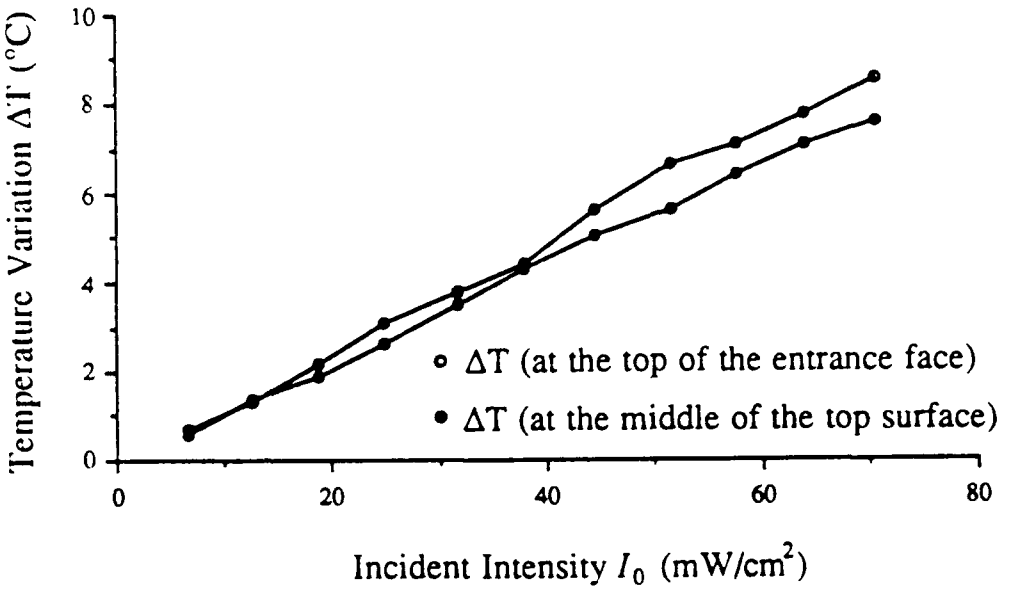

Figure 2

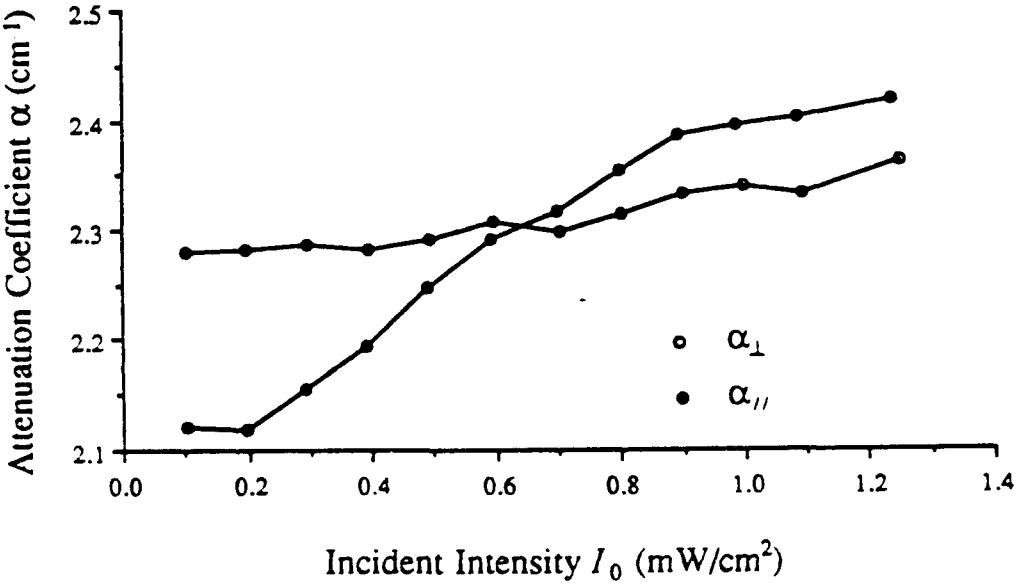

Figure 3

(a)

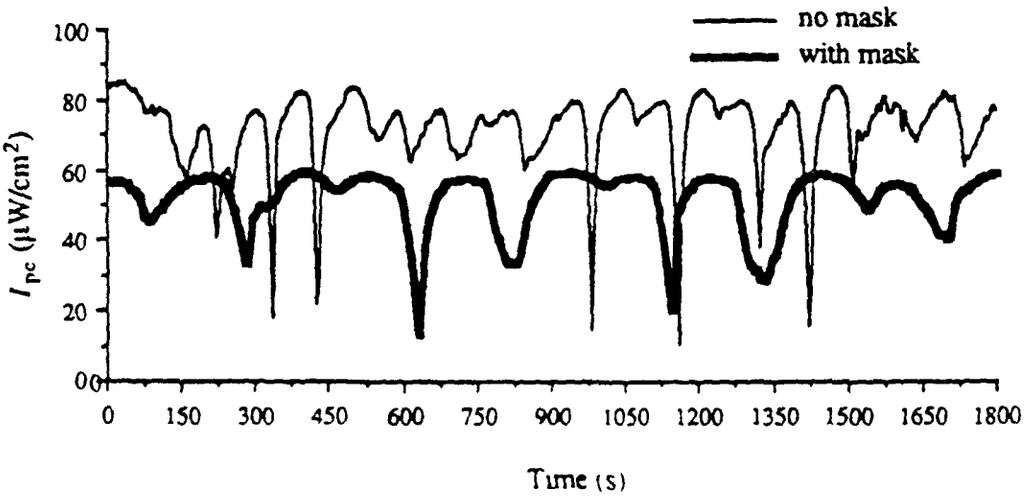
no mask
with mask
100
80
60
40
20
00
I_{pc} (μW/cm^2)
0
150
300
450
600
750
900
1050
1200
1350
1500
1650
1800
Time (s)

(b)

Figure 4

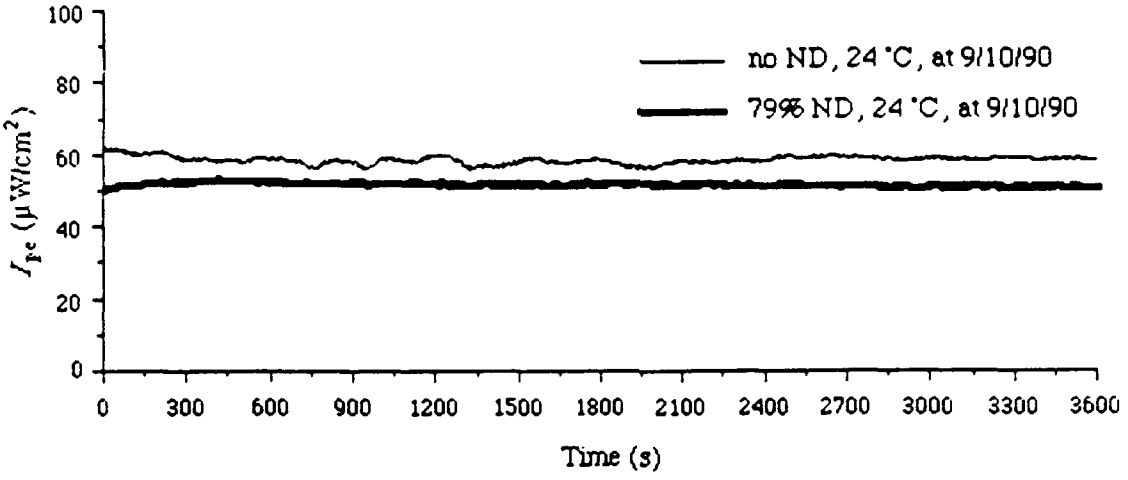
100
80
60
40
20
0
I_{Fe} (μW/cm^2)
no ND, 24 °C, at 9/10/90
79% ND, 24 °C, at 9/10/90
0
300
600
900
1200
1500
1800
2100
2400
2700
3000
3300
3600
Time (s)

Figure 5

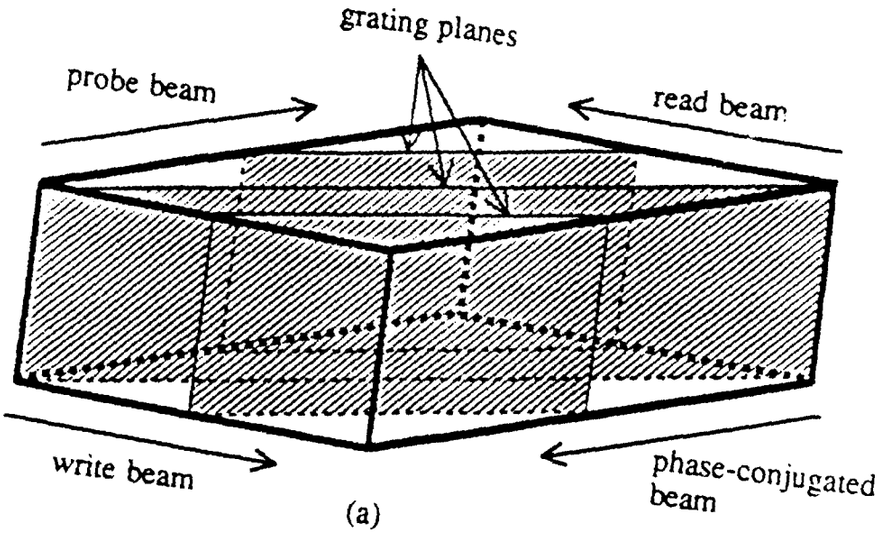
grating planes
probe beam
read beam
write beam
phase-conjugated beam

(a)

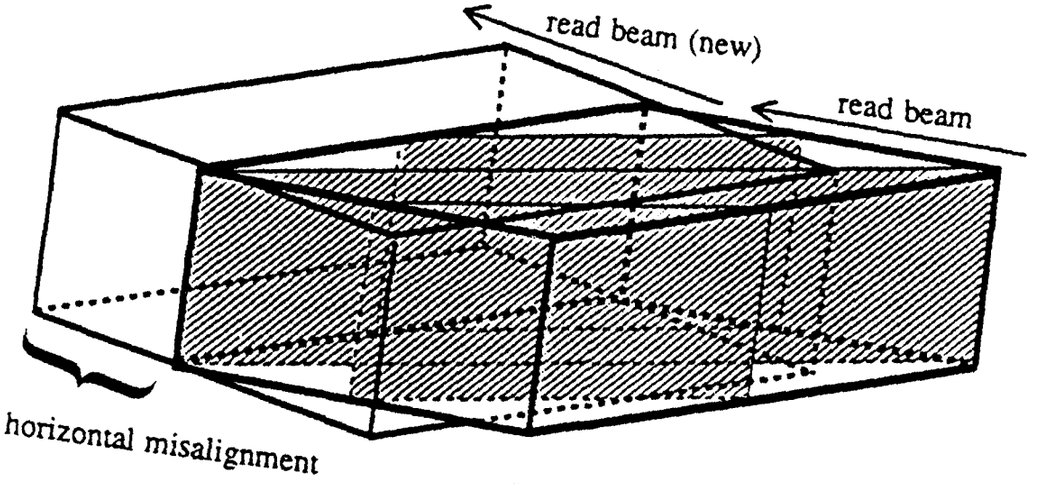
read beam (new)
read beam
horizontal misalignment

(b)

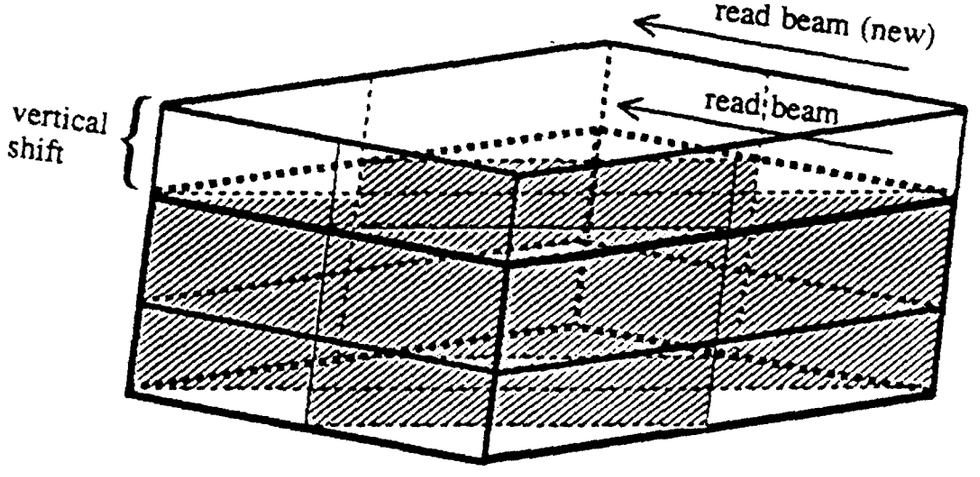
read beam (new)
read beam
vertical shift

(c)

Figure 6

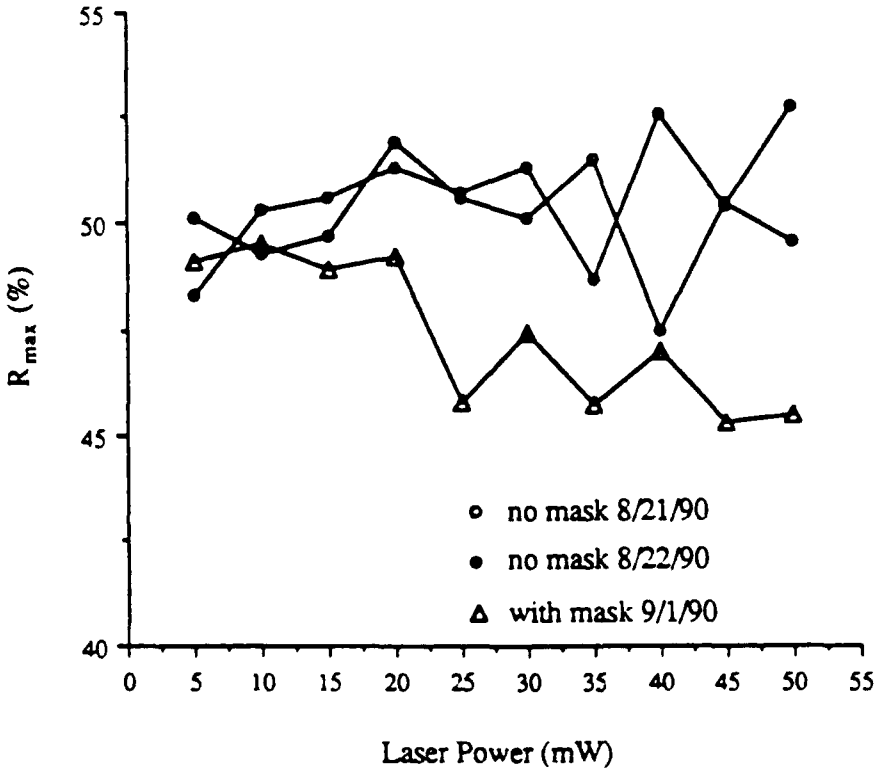
55
50
45
40
R_{max} (%)
0
5
10
15
20
25
30
35
40
45
50
55
Laser Power (mW)
no mask 8/21/90
no mask 8/22/90
with mask 9/1/90

Figure 7

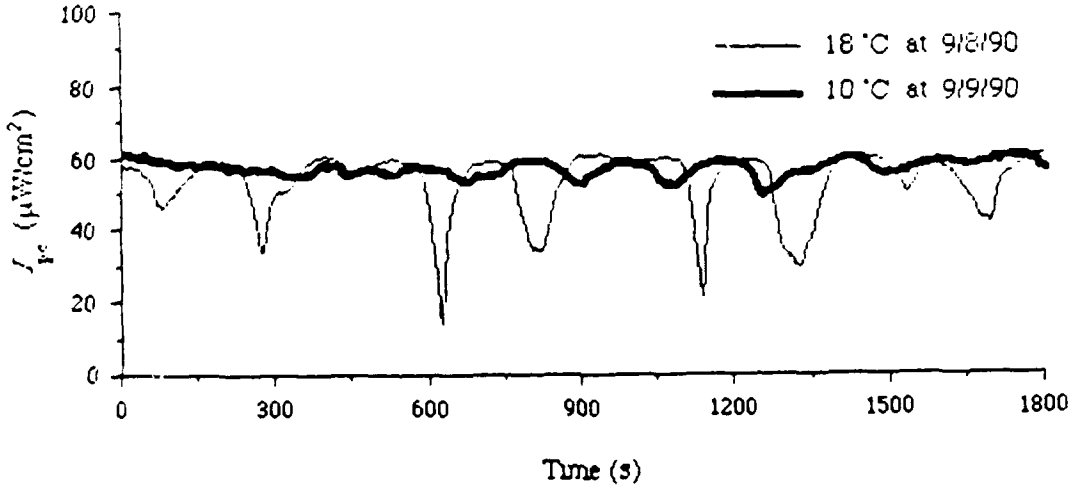
18 °C at 9/8/90
10 °C at 9/9/90
100
80
60
40
20
0
0
300
600
900
1200
1500
1800
Time (s)

(a)

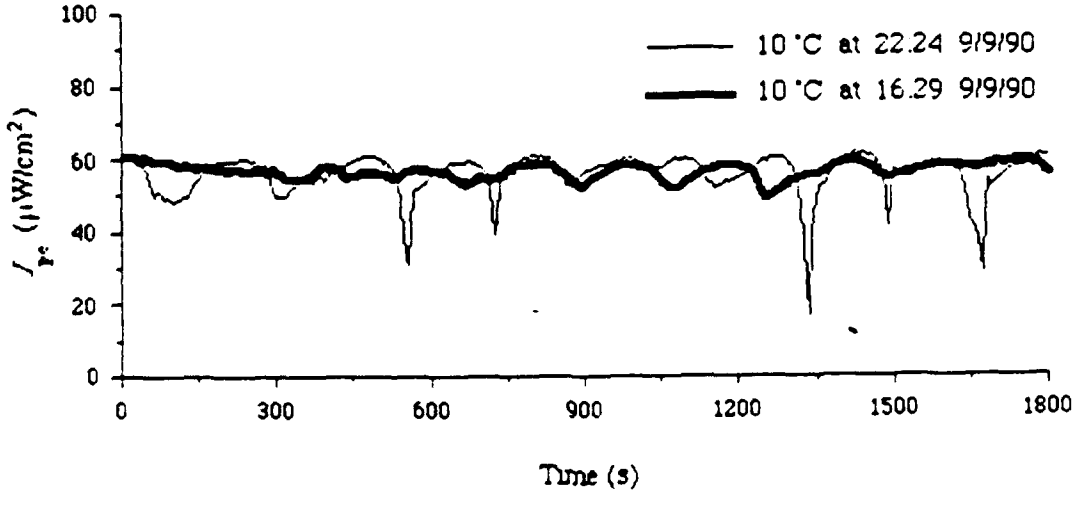
10 °C at 22.24 9/9/90
10 °C at 16.29 9/9/90
100
80
60
40
20
0
0
300
600
900
1200
1500
1800
Time (s)

(b)

Figure 8